Supplementary Material for Learning Neural Implicit through Volume Rendering with Attentive Depth Fusion Priors

Pengchong Hu **Zhizhong Han**
Machine Perception Lab, Wayne State University, Detroit, USA

1 Implementation Details

In all of our experiments, the voxel size of the low resolution feature grid G_l and the high resolution feature grid G_h is set to 0.32 and 0.16, respectively. The voxel size of the color feature grid G_c is the same as the one in G_h. For the TSDF G_s, we use a resolution that produces a voxel size of $\frac{1}{64}$. All of the feature vectors in the feature grids have the same dimension $d = 32$.

All MLP decoders have 5 fully-connected blocks, each of which produces a hidden feature dimension of 32. For the pre-trained decoder f_l and f_h, we follow the same process and setting as NICE-SLAM [21] during pre-training. Note that the input feature vectors of decoder f_h consist of the interpolated feature vectors from G_l and G_h. For the neural function f_a, we use an MLP with 6 fully-connected layers, and a Softmax layer that can normalize the output weights α and β.

For experiments on Replica [10], we shoot $K = 1000$ rays for reconstruction and $K_t = 200$ rays for camera tracking from each view. For experiments on ScanNet [1], we use $K = 5000$ for reconstruction and $K_t = 1000$ for camera tracking from each view. During the optimizing process, the learning rate for optimizing low frequency feature grid G_l is $1e - 1$, for optimizing both low and high frequency feature grid G_l and G_h is $5e - 3$, and for optimizing G_l, G_h, and G_c jointly is $5e - 3$. The learning rate for tracking on Replica [10] and ScanNet [1] are set to $1e - 3$ and $5e - 3$, respectively. The learning rate for color decoder f_c and neural function f_a are set to $5e - 3$ and $5e - 6$, respectively. For optimizing scene geometry, we use 60 iterations on Replica [10] and ScanNet [1]. For optimizing camera tracking, we use 10 iterations and 50 iterations on Replica [10] and ScanNet [1], respectively.

For experiments in the context of SLAM, we will maintain two TSDF volumes T and T_{temp} for the streaming fusion. After the tracking procedure at time step t, the after-fusion stage first fuses the t-th depth image into T that has fused all depth images in front using the estimated t-th camera pose. Then, we make a copy of T and send it to T_{temp}. The pre-fusion stage will fuse the $t + 1$-th depth image into T_{temp} using the camera pose estimated based on constant speed assumption. After that, T_{temp} will be used in tracking procedure to get an updated $t + 1$-th camera pose, with which T can be updated by fusing the $t + 1$-th depth image.

2 More Results

Beyond the average results in our paper, we report more detailed results in Tab. 1 and Tab. 2 on Replica [10] and ScanNet [1]. We compare with the latest methods on each scene that we used in evaluations in terms of the same metrics as the previous methods. We can see that our method predicts more accurate geometry than the latest methods on most of scenes. In Tab. 1, we report our results with estimated camera poses as "Ours" and also the results with GT camera poses as "Ours*", where all compared methods are reported with estimated camera poses except for vMAP [5]. Meanwhile, we report our methods with GT camera poses in Tab. 2. The comparisons show that our method can more effectively leverage depth priors to learn neural implicit from RGBD images.

37th Conference on Neural Information Processing Systems (NeurIPS 2023).

Table 1: Reconstruction Comparisons on Replica.

		room-0	room-1	room-2	office-0	office-1	office-2	office-3	office-4	Avg.
COLMAP [9]	**Depth L1** [cm] $\downarrow$	-	-	-	-	-	-	-	-	-
	Acc. [cm] $\downarrow$	3.87	27.29	5.41	5.21	12.69	4.28	5.29	5.45	8.69
	Comp. [cm] $\downarrow$	4.78	23.90	17.42	12.98	12.35	4.96	16.17	4.41	12.12
	Comp. Ratio [< 5 cm%] $\uparrow$	83.08	22.89	64.47	72.59	69.52	81.12	64.38	82.92	67.62
TSDF-Fusion [19]	**Depth L1** [cm] $\downarrow$	4.17	6.67	6.60	3.23	4.71	11.59	9.02	6.48	6.56
	Acc. [cm] $\downarrow$	1.63	1.49	1.37	1.23	1.02	2.11	2.01	1.65	**1.56**
	Comp. [cm] $\downarrow$	3.78	3.41	3.11	1.92	2.54	3.87	3.77	4.27	3.33
	Comp. Ratio [< 5 cm%] $\uparrow$	87.59	88.75	88.87	92.30	89.00	85.21	84.78	84.40	87.61
iMAP [11]	**Depth L1** [cm] $\downarrow$	5.70	4.93	6.94	6.43	7.41	14.23	8.68	6.80	7.64
	Acc. [cm] $\downarrow$	5.66	5.31	5.64	7.39	11.89	8.12	5.62	5.98	6.95
	Comp. [cm] $\downarrow$	5.20	5.16	5.04	4.35	5.00	6.33	5.47	6.10	5.33
	Comp. Ratio [< 5 cm%] $\uparrow$	67.67	66.41	69.27	71.97	71.58	58.31	65.95	61.64	66.60
DI-Fusion [4]	**Depth L1** [cm] $\downarrow$	6.66	96.82	36.09	7.36	5.05	13.73	11.41	9.55	23.33
	Acc. [cm] $\downarrow$	1.79	49.00	26.17	70.56	1.42	2.11	2.11	2.02	19.40
	Comp. [cm] $\downarrow$	3.57	39.40	17.35	3.58	2.20	4.83	4.71	5.84	10.19
	Comp. Ratio [< 5 cm%] $\uparrow$	87.77	32.01	45.61	87.17	91.85	80.13	78.94	80.21	72.96
NICE-SLAM [21]	**Depth L1** [cm] $\downarrow$	2.11	1.68	2.90	1.83	2.46	8.92	5.93	2.38	3.53
	Acc. [cm] $\downarrow$	2.73	2.58	2.65	2.26	2.50	3.82	3.50	2.77	2.85
	Comp. [cm] $\downarrow$	2.87	2.47	3.00	2.02	2.36	3.57	3.83	3.84	3.00
	Comp. Ratio [< 5 cm%] $\uparrow$	90.93	92.80	89.07	94.93	92.61	85.20	82.98	86.14	89.33
Vox-Fusion [16]	**Depth L1** [cm] $\downarrow$	-	-	-	-	-	-	-	-	-
	Acc. [cm] $\downarrow$	2.53	1.69	3.33	2.20	2.21	2.72	4.16	2.48	2.67
	Comp. [cm] $\downarrow$	2.81	2.51	4.03	8.75	7.36	4.519	3.26	3.49	4.55
	Comp. Ratio [< 5 cm%] $\uparrow$	91.52	91.34	86.78	81.99	82.03	85.45	87.13	86.53	86.59
DROID-SLAM [12]	**Depth L1** [cm] $\downarrow$	-	-	-	-	-	-	-	-	-
	Acc. [cm] $\downarrow$	12.18	8.35	3.26	3.01	2.39	5.66	4.49	4.65	5.50
	Comp. [cm] $\downarrow$	8.96	6.07	16.01	16.19	16.20	15.56	9.73	9.63	12.29
	Comp. Ratio [< 5 cm%] $\uparrow$	60.07	76.20	61.62	64.19	60.63	56.78	61.95	67.51	63.62
NICER-SLAM [20]	**Depth L1** [cm] $\downarrow$	-	-	-	-	-	-	-	-	-
	Acc. [cm] $\downarrow$	2.53	3.93	3.40	5.49	3.45	4.02	3.34	3.03	3.65
	Comp. [cm] $\downarrow$	3.04	4.10	3.42	6.09	4.42	4.29	4.03	3.87	4.16
	Comp. Ratio [< 5 cm%] $\uparrow$	88.75	76.61	86.10	65.19	77.84	74.51	82.01	83.98	79.37
Ours	**Depth L1** [cm] $\downarrow$	1.44	1.90	2.75	1.43	2.03	7.73	4.81	1.99	**3.01**
	Acc. [cm] $\downarrow$	2.54	2.70	2.25	2.14	2.80	3.58	3.46	2.68	2.77
	Comp. [cm] $\downarrow$	2.41	2.26	2.46	1.76	1.94	2.56	2.93	3.27	**2.45**
	Comp. Ratio [< 5 cm%] $\uparrow$	93.22	94.75	93.02	96.04	94.77	91.89	90.17	88.46	**92.79**
vMAP [5]	**Depth L1** [cm] $\downarrow$	-	-	-	-	-	-	-	-	-
	Acc. [cm] $\downarrow$	2.77	3.87	1.83	4.82	3.51	3.35	3.19	2.26	3.20
	Comp. [cm] $\downarrow$	1.99	1.81	2.00	3.65	2.14	2.45	2.49	2.56	2.39
	Comp. Ratio [< 5 cm%] $\uparrow$	97.10	96.59	95.72	87.53	85.08	94.70	93.65	93.56	92.99
Ours*	**Depth L1** [cm] $\downarrow$	1.05	0.91	1.54	0.91	1.37	8.21	5.52	1.25	**2.60**
	Acc. [cm] $\downarrow$	2.59	2.27	2.03	2.33	2.56	3.32	3.23	2.42	**2.59**
	Comp. [cm] $\downarrow$	2.41	1.89	2.00	1.49	1.78	2.51	3.08	3.09	**2.28**
	Comp. Ratio [< 5 cm%] $\uparrow$	93.45	94.87	94.51	96.88	94.55	92.10	90.78	89.88	**93.38**

One thing about the fairness that is worth mentioning in the comparisons is that we follow the SLAM setting and regard the images as a view sequence and only use images that are in front of the current view to infer the neural implicit although we know GT camera poses in Tab. 2. While other methods including UNISURF [8], NeuS [15], VolSDF [17], MonoSDF [18], GO-Surf [13] can use all images at the same time. The information difference makes our method not able to observe the whole scene at the same time. But our attentive depth prior alleviates this demerit, which still leads us to produce better results than the latest methods requiring all images to infer the implicit scene representations.

Additionally, for fair comparisons with MonoSDF [18], we also use GT depth maps to report their results on ScanNet in Tab. 3 and Fig. 3. However, the improvement from GT depth maps is marginal, which is still not as good as ours. We did intend to use the estimated depth images to produce our results. However, we found each estimated depth image used by MonoSDF [18] needs a pair of scale and shift parameters to get normalized, which aligns the estimated point cloud to the scene surface. However, the scale and shift parameters are not consistent across different views, which makes it hard to fuse the estimated depth images into a plausible TSDF, even if using GT camera poses. Fig. 1 shows that the TSDF fails to represent a coarse structure of the scene, which can not be used as a depth fusion prior in our method. Meanwhile, compared to FastSurf [6] that directly uses the TSDF as supervision and can only work in multi- view reconstruction but not SLAM, we report better results in Tab. 4 and Fig. 4.

We also report visual comparisons with data-driven or hole filling methods such as SG-NN [2] and Filling Holes in Meshes [7] in Fig. 2 in the rebuttal. SG-NN fails to fill holes in the scene with ceilings, and [7] produces severe artifacts in empty space due to its limited ability of perceiving the context.

Table 2: Reconstruction Comparisons on ScanNet.

		Acc ↓	Comp ↓	Chamfer-L_1 ↓	Prec ↑	Recall ↑	F-score ↑
scene 0050	COLMAP [9]	0.059	0.174	0.117	0.659	0.491	0.563
	UNISURF [8]	0.485	0.102	0.294	0.258	0.432	0.323
	NeuS [15]	0.130	0.115	0.123	0.441	0.406	0.423
	VolSDF [17]	0.092	0.079	0.086	0.512	0.544	0.527
	Manhattan-SDF [3]	0.058	0.059	0.059	0.707	0.642	0.673
	NeuRIS [14]	-	-	-	-	-	-
	MonoSDF [18]	-	-	-	-	-	-
	GO-Surf [13]	0.056	0.024	0.040	0.911	0.919	0.915
	NICE-SLAM [21]	0.030	0.053	0.041	0.930	0.816	0.869
	Ours	0.030	0.043	0.037	0.958	0.898	0.927
scene 0084	COLMAP [9]	0.042	0.134	0.088	0.736	0.552	0.631
	UNISURF [8]	0.638	0.247	0.762	0.189	0.326	0.239
	NeuS [15]	0.255	0.360	0.308	0.128	0.084	0.101
	VolSDF [17]	0.551	0.162	0.357	0.127	0.232	0.164
	Manhattan-SDF [3]	0.055	0.053	0.054	0.639	0.621	0.630
	NeuRIS [14]	-	-	-	-	-	-
	MonoSDF [18]	-	-	-	-	-	-
	GO-Surf [13]	0.073	0.017	0.045	0.931	0.981	0.955
	NICE-SLAM [21]	0.031	0.020	0.025	0.945	0.929	0.937
	Ours	0.039	0.014	0.026	0.924	0.963	0.943
scene 0580	COLMAP [9]	0.034	0.176	0.105	0.809	0.465	0.590
	UNISURF [8]	0.376	0.116	0.246	0.218	0.399	0.282
	NeuS [15]	0.161	0.215	0.188	0.413	0.327	0.365
	VolSDF [17]	0.091	0.088	0.090	0.529	0.540	0.534
	Manhattan-SDF [3]	0.104	0.062	0.153	0.616	0.650	0.632
	NeuRIS [14]	-	-	-	-	-	-
	MonoSDF [18]	-	-	-	-	-	-
	GO-Surf [13]	0.057	0.024	0.040	0.911	0.920	0.915
	NICE-SLAM [21]	0.032	0.031	0.032	0.939	0.888	0.913
	Ours	0.041	0.035	0.038	0.824	0.875	0.849
scene 0616	COLMAP [9]	0.054	0.457	0.256	0.638	0.256	0.365
	UNISURF [8]	0.716	0.193	0.455	0.183	0.293	0.225
	NeuS [15]	0.171	0.142	0.157	0.269	0.284	0.276
	VolSDF [17]	0.922	0.150	0.536	0.115	0.259	0.160
	Manhattan-SDF [3]	0.072	0.098	0.085	0.521	0.431	0.472
	NeuRIS [14]	-	-	-	-	-	-
	MonoSDF [18]	-	-	-	-	-	-
	GO-Surf [13]	0.026	0.023	0.025	0.939	0.894	0.916
	NICE-SLAM [21]	0.026	0.076	0.051	0.935	0.764	0.841
	Ours	0.026	0.063	0.045	0.945	0.840	0.889

Table 3: Reconstruction Comparisons with MonoSDF on ScanNet (scene 0050).

	Acc ↓	Comp ↓	CD-L_1 ↓	Prec ↑	Recall ↑	F-score ↑
Predict	0.041	0.054	0.048	0.722	0.621	0.667
GT	0.039	0.049	0.044	0.763	0.682	0.721
Ours	**0.030**	**0.043**	**0.037**	**0.958**	**0.898**	**0.927**

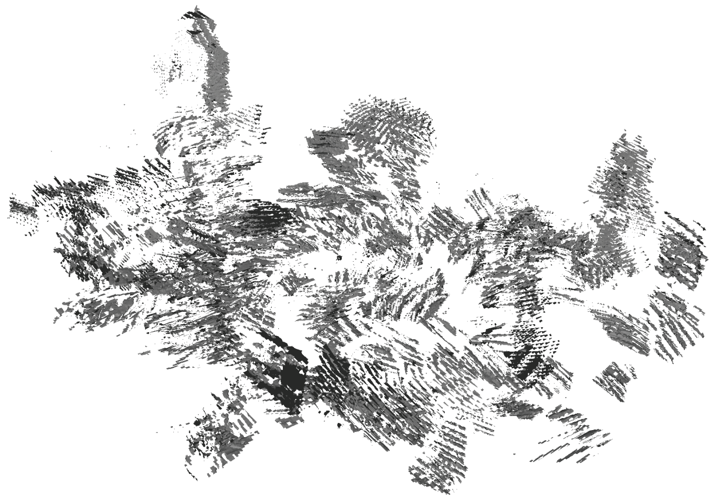

Figure 1: Visualization of TSDF(estimated depth).

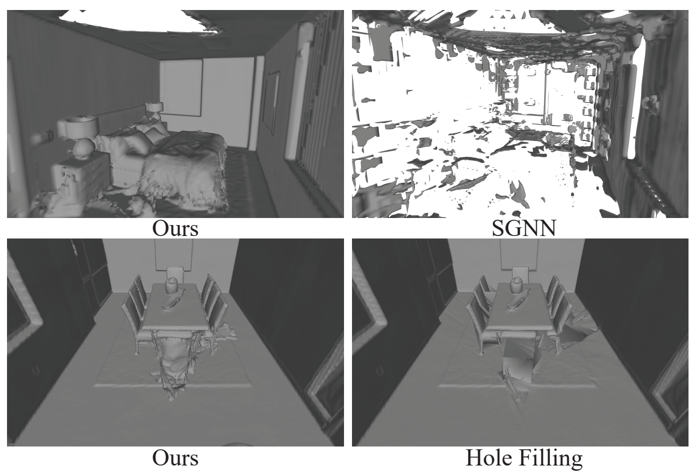

Figure 2: Visual comparisons with hole filling methods.

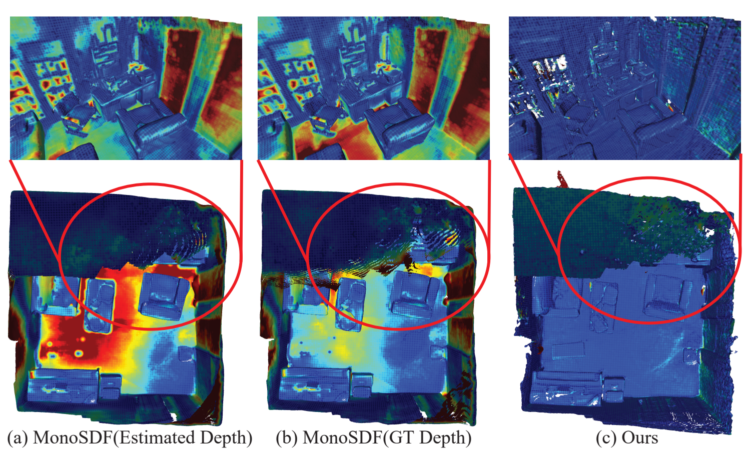

Figure 3: Visual comparisons of error maps (Red: Large) with MonoSDF.

Table 4: Reconstruction Comparisons with FastSurf on ScanNet.

Scene ID		Acc ↓	Comp ↓	CD-L_1 ↓	Prec ↑	Recall ↑	F-score ↑
0002	FS25K	**0.033**	0.053	0.043	0.855	0.684	0.760
	FS75K	**0.033**	0.057	0.046	0.819	0.655	0.728
	Ours	**0.033**	**0.026**	**0.029**	**0.889**	**0.875**	**0.882**
0005	FS25K	0.098	0.056	0.077	0.654	0.658	0.656
	FS75K	0.099	0.057	0.088	0.621	0.622	0.621
	Ours	**0.097**	**0.024**	**0.061**	**0.776**	**0.926**	**0.844**
0050	FS25K	0.042	0.048	0.045	0.657	0.616	0.636
	FS75K	0.042	0.048	0.045	0.670	0.625	0.647
	Ours	**0.030**	**0.043**	**0.037**	**0.958**	**0.898**	**0.927**

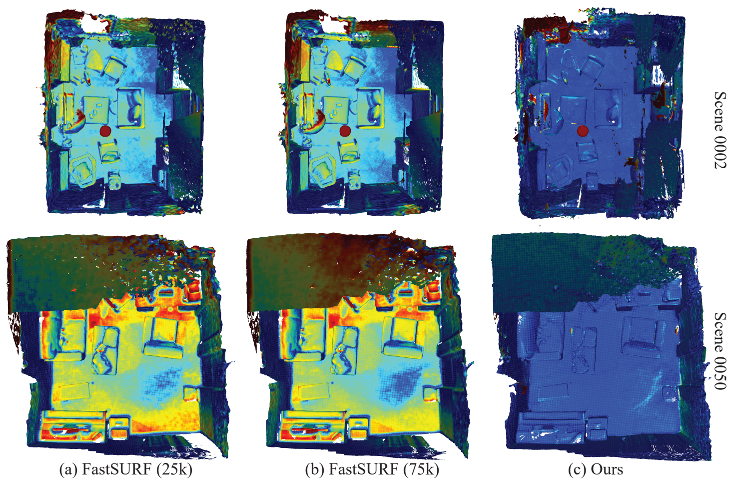

Figure 4: Visual comparisons of error maps (Red: Large) with FastSurf.

Table 5: Ablation Studies on Depth Priors.

	NICE-SLAM [21] GT+w/o depth loss	Ours GT+w/o depth loss	NICE-SLAM [21]	Ours
Depth L1 [cm] ↓	38.11	**12.82**	2.11	**1.44**
Acc. [cm] ↓	18.29	**8.49**	2.73	**2.54**
Comp. [cm] ↓	11.13	**3.48**	2.87	**2.41**
Comp. Ratio [<5 cm%] ↑	41.47	**91.35**	90.93	**93.22**

3 More Ablation Studies

Beyond the ablation studies in our paper, we report more ablation studies to highlight the effectiveness of using depth fusion priors. As a more effective way of using depth priors than rendering single depth images, we compare the results with or without rendering depth images. Specifically, we use NICE-SLAM [21] as a baseline, and show its results with or without the depth rendering loss during the mapping procedure in Fig. 5. We use the GT camera poses to ensure that inaccurate camera poses do not affect the performance. We keep the experimental setup the same as NICE-SLAM [21], but use our attentive depth prior in our results.

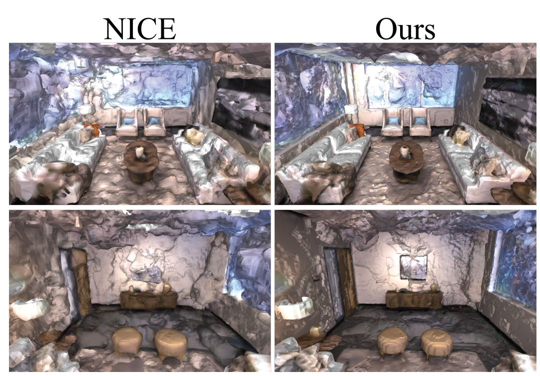

Figure 5: Demonstration of the effect of depth loss.

Tab. 5 shows that our attentive depth prior can help network to leverage the depth information with or without using depth rendering loss. Moreover, our attentive depth prior can play a more important

Table 6: Ablation Studies on Attention Alternatives.

		w/o mlp	max	Feature	Ours
room0	**Acc.** ↓	2.88	2.65	2.66	**2.59**
	Comp. ↓	2.74	2.47	2.46	**2.41**
	Comp. Ratio ↑	92.70	92.84	93.39	**93.45**
office0	**Acc.** ↓	2.75	2.56	2.41	**2.33**
	Comp. ↓	2.03	1.88	1.69	**1.49**
	Comp. Ratio ↑	95.236	95.57	96.10	**96.88**

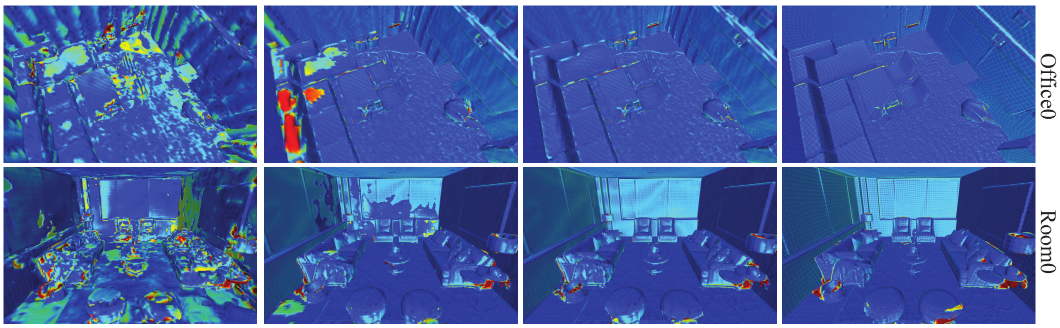

(a) Softmax without MLP (b) Occupancy with maximum weight (c) Using features as additional conditions (d) Ours

Figure 6: Visual comparison of error maps with different attention alternatives (Red: Large).

role to perceive the 3D structure if there is no depth rendering loss used. We also present a visual comparison in Fig. 5 to show the reconstructions of NICE-SLAM [21] and ours without using the depth rendering loss. We can see that our attentive depth priors can significantly improve the reconstruction performance.

Beyond the ablation study about attentive alternatives introduced in main text, we also conduct experiments to report more results with different conditions in Tab. 6 and Fig. 6. All these alternatives degenerate the reconstruction accuracy. Specifically, we remove the MLP and just use a softmax to normalize the two occupancy inputs in Fig. 6(a), use the occupancy with the maximum weight in Fig. 6(b), and use more conditions as input including the features of points that are interpolated from the low and high resolution feature grids in Fig. 6(c).

4 More Visualizations

We show more visualizations to present our learning procedure.

Reconstruction. First of all, we visualize the learning procedure for reconstruction. We visualize the reconstructed meshes using the occupancy function f learned during training in Fig. 7. To highlight our advantages over NICE-SLAM [21], we also show error maps on reconstructed meshes. We can see that we can learn more accurate implicit functions than NICE-SLAM [21] with our attentive depth fusion prior in different iterations. Please watch our video for more visualization of the reconstruction process.

Attention. Then, we visualize the effect of our attention mechanism during our learning procedure. With our attention mechanism, our neural network is able to select better geometry clues at different locations for the learning of implicit representations. In Fig. 8, we visualize the attention weights for the TSDF G_s on a cross section through a scene during training. The attention weights are learned progressively to achieve a stable state so that we can render depth and RGB images that are similar to the ground truth.

View Rendering. We compare the rendered RGB and depth images with NICE-SLAM [21] in Fig. 9. The visual comparisons show that our attentive depth fusion prior can also improve the rendering quality. This is also a merit for novel view synthesis.

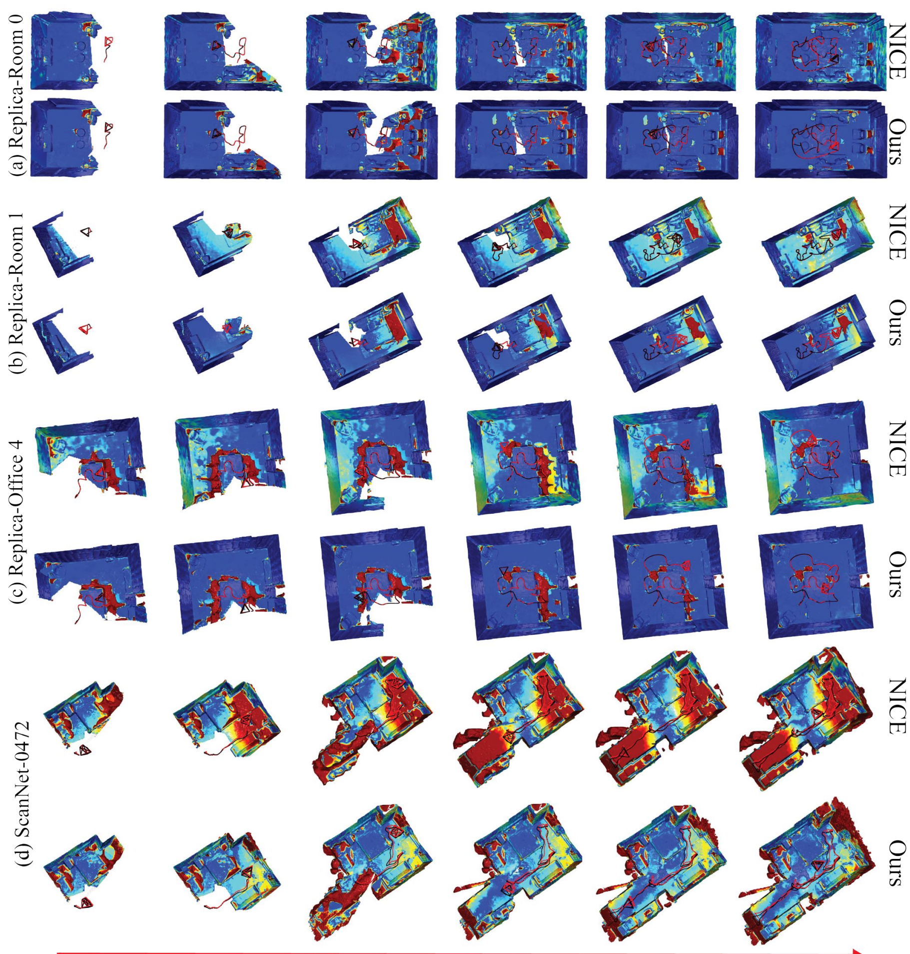

Figure 7: Visual comparisons of error maps (Red: Large) during surface reconstructions on Replica and ScanNet.

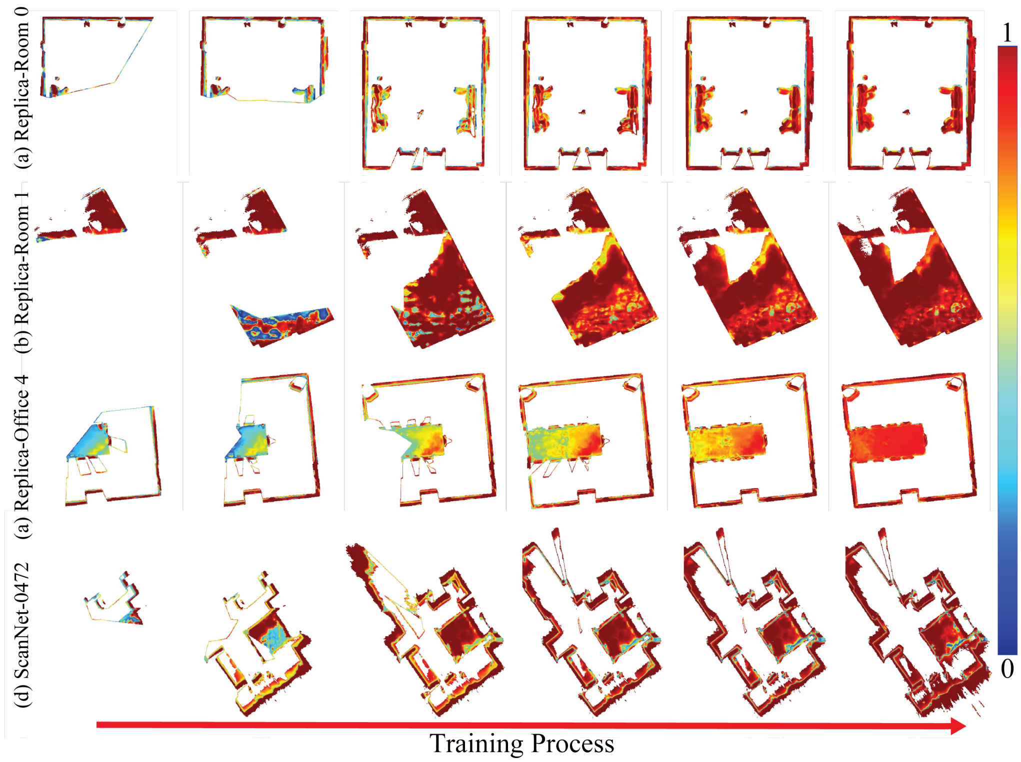

Figure 8: Visualization of attention (Red: Large) on the TSDF G_s during neural implicit inference on Replica and ScanNet.

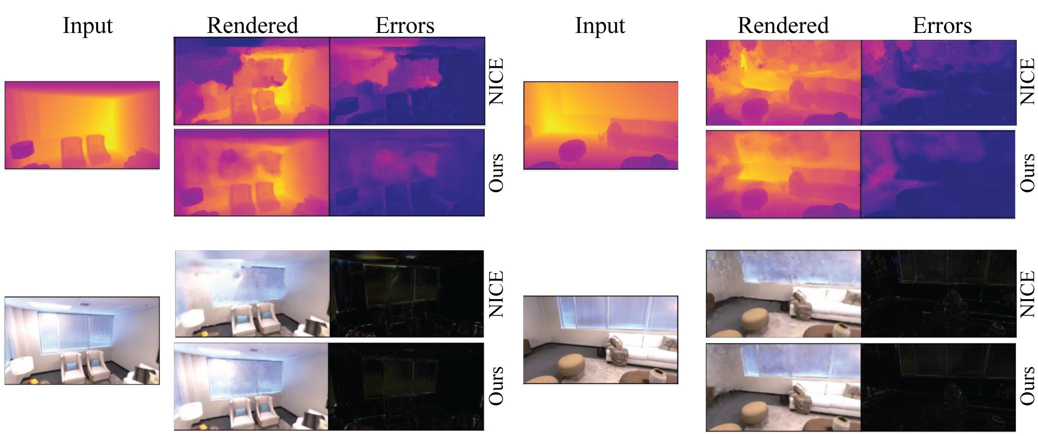

Figure 9: Visual comparisons of rendered images with NICE-SLAM.

References

[1] Angela Dai, Angel X. Chang, Manolis Savva, Maciej Halber, Thomas A. Funkhouser, and Matthias Nießner. Scannet: Richly-annotated 3d reconstructions of indoor scenes. *CoRR*, abs/1702.04405, 2017.

[2] Angela Dai, Christian Diller, and Matthias Nießner. SG-NN: Sparse generative neural networks for self-supervised scene completion of rgb-d scans. *ArXiv*, abs/1912.00036, 2019.

[3] Haoyu Guo, Sida Peng, Haotong Lin, Qianqian Wang, Guofeng Zhang, Hujun Bao, and Xiaowei Zhou. Neural 3d scene reconstruction with the manhattan-world assumption. In *IEEE Conference on Computer Vision and Pattern Recognition*, 2022.

[4] Jiahui Huang, Shi-Sheng Huang, Haoxuan Song, and Shi-Min Hu. Di-fusion: Online implicit 3d reconstruction with deep priors, 2021.

[5] Xin Kong, Shikun Liu, Marwan Taher, and Andrew J Davison. vmap: Vectorised object mapping for neural field slam. *arXiv preprint arXiv:2302.01838*, 2023.

[6] Seunghwan Lee, Gwanmo Park, Hyewon Son, Jiwon Ryu, and Han Joo Chae. Fastsurf: Fast neural rgb-d surface reconstruction using per-frame intrinsic refinement and tsdf fusion prior learning. *arXiv preprint arXiv:2303.04508*, 2023.

[7] Peter Liepa. Filling holes in meshes. In *Proceedings of the 2003 Eurographics/ACM SIGGRAPH Symposium on Geometry Processing*, SGP '03, page 200–205, Goslar, DEU, 2003. Eurographics Association.

[8] Michael Oechsle, Songyou Peng, and Andreas Geiger. UNISURF: Unifying neural implicit surfaces and radiance fields for multi-view reconstruction. In *International Conference on Computer Vision*, 2021.

[9] Johannes Lutz Schönberger, Enliang Zheng, Marc Pollefeys, and Jan-Michael Frahm. Pixelwise view selection for unstructured multi-view stereo. In *European Conference on Computer Vision*, 2016.

[10] Julian Straub, Thomas Whelan, Lingni Ma, Yufan Chen, Erik Wijmans, Simon Green, Jakob J. Engel, Raul Mur-Artal, Carl Ren, Shobhit Verma, Anton Clarkson, Mingfei Yan, Brian Budge, Yajie Yan, Xiaqing Pan, June Yon, Yuyang Zou, Kimberly Leon, Nigel Carter, Jesus Briales, Tyler Gillingham, Elias Mueggler, Luis Pesqueira, Manolis Savva, Dhruv Batra, Hauke M. Strasdat, Renzo De Nardi, Michael Goesele, Steven Lovegrove, and Richard A. Newcombe. The replica dataset: A digital replica of indoor spaces. *CoRR*, abs/1906.05797, 2019.

[11] Edgar Sucar, Shikun Liu, Joseph Ortiz, and Andrew J Davison. imap: Implicit mapping and positioning in real-time. In *Proceedings of the IEEE/CVF International Conference on Computer Vision*, pages 6229–6238, 2021.

[12] Zachary Teed and Jia Deng. DROID-SLAM: Deep Visual SLAM for Monocular, Stereo, and RGB-D Cameras. *Advances in neural information processing systems*, 2021.

[13] Jingwen Wang, Tymoteusz Bleja, and Lourdes Agapito. Go-surf: Neural feature grid optimization for fast, high-fidelity rgb-d surface reconstruction. In *International Conference on 3D Vision*, 2022.

[14] Jiepeng Wang, Peng Wang, Xiaoxiao Long, Christian Theobalt, Taku Komura, Lingjie Liu, and Wenping Wang. NeuRIS: Neural reconstruction of indoor scenes using normal priors. In *European Conference on Computer Vision*, 2022.

[15] Peng Wang, Lingjie Liu, Yuan Liu, Christian Theobalt, Taku Komura, and Wenping Wang. NeuS: Learning neural implicit surfaces by volume rendering for multi-view reconstruction. In *Advances in Neural Information Processing Systems*, pages 27171–27183, 2021.

[16] Xingrui Yang, Hai Li, Hongjia Zhai, Yuhang Ming, Yuqian Liu, and Guofeng Zhang. Vox-fusion: Dense tracking and mapping with voxel-based neural implicit representation. In *2022 IEEE International Symposium on Mixed and Augmented Reality (ISMAR)*, Dec 2022.

[17] Lior Yariv, Jiatao Gu, Yoni Kasten, and Yaron Lipman. Volume rendering of neural implicit surfaces. In *Advances in Neural Information Processing Systems*, 2021.

[18] Zehao Yu, Songyou Peng, Michael Niemeyer, Torsten Sattler, and Andreas Geiger. MonoSDF: Exploring monocular geometric cues for neural implicit surface reconstruction. *ArXiv*, abs/2022.00665, 2022.

[19] Andy Zeng, Shuran Song, Matthias Nießner, Matthew Fisher, Jianxiong Xiao, and Thomas Funkhouser. 3dmatch: Learning local geometric descriptors from rgb-d reconstructions. In *CVPR*, 2017.

[20] Zihan Zhu, Songyou Peng, Viktor Larsson, Zhaopeng Cui, Martin R. Oswald, Andreas Geiger, and Marc Pollefeys. NICER-SLAM: neural implicit scene encoding for RGB SLAM. *CoRR*, abs/2302.03594, 2023.

[21] Zihan Zhu, Songyou Peng, Viktor Larsson, Weiwei Xu, Hujun Bao, Zhaopeng Cui, Martin R. Oswald, and Marc Pollefeys. Nice-slam: Neural implicit scalable encoding for slam. In *IEEE Conference on Computer Vision and Pattern Recognition*, 2022.